Journal of Hazardous Materials 221–222 (2012) 298–302

Contents lists available at SciVerse ScienceDirect

Journal of Hazardous Materials

journal homepage: www.elsevier.com/locate/jhazmat

Short communication

Reliability of chemical microanalyses for solid waste materials

Vojtěch Ettler[a,*], Zdenek Johan[b], Martina Vítková[a], Roman Skála[a,c], Marek Kotrlý[d], Gerlinde Habler[e], Mariana Klementová[f]

[a] Institute of Geochemistry, Mineralogy and Mineral Resources, Charles University in Prague, Faculty of Science, Albertov 6, 128 43 Prague 2, Czech Republic
[b] Bureau des Recherches Géologiques et Minières (BRGM), av. Claude Guillemin, 45060 Orléans, Cedex 2, France
[c] Institute of Geology of the ASCR, v.v.i., Rozvojová 269, 165 00 Prague 6, Czech Republic
[d] Institute of Criminalistics Prague, P.O. Box 62/KUP, Strojnická 27, 170 89 Prague 7, Czech Republic
[e] Department of Lithospheric Research, University of Vienna, Althanstrasse 14, A-1090 Vienna, Austria
[f] Institute of Inorganic Chemistry of the AS CR, v.v.i., 250 68 Husinec-Řež, Czech Republic

ARTICLE INFO

Article history:
Received 30 September 2011
Received in revised form 3 April 2012
Accepted 6 April 2012
Available online 13 April 2012

Keywords:
Solid speciation
Contaminants
Electron probe microanalysis
FIB-TEM
Slag

ABSTRACT

The investigation of solid speciation of metals and metalloids is required for accurate assessment of the hazardous properties of solid waste materials from high-temperature technologies (slag, bottom ash, fly ash, air-pollution-control residues). This paper deals with the problem of reliability of microanalyses using a combination of electron microprobe analysis (EPMA) and scanning electron microscopy (SEM) only. These methods do not permit to detect nanophases in host-crystals and lead to erroneous interpretation of analytical results, considering the elements of nanophases as belonging to the crystal structure of the main phase. More detailed analysis using transmission electron microscopy (TEM) on foils prepared by focused ion beam (FIB) can be used to solve this analytical problem. In this study, lamellar aggregates of potassium-rich clinopyroxenes were detected in copper smelting slags by a combination of SEM and EPMA. However, FIB-TEM indicated the presence of leucite inclusions (tens to hundreds nm in size) within the clinopyroxene lamellae. Based on examples from smelting slags and other solid waste materials, recommendations for standard SEM and EPMA applications and the need for methods with higher resolution for mineralogical investigation of waste materials are discussed.

1. Introduction

The knowledge of detailed mineralogical and chemical compositions of solid phases is crucial for the assessment of hazardous properties in solid waste materials [1]. During the past decade, an increasing number of papers has been devoted to mineralogical investigations of waste materials from numerous high-temperature technologies, including metallurgical slags and mattes [2–13], bottom and fly ashes from municipal solid waste incinerators (MSWI) [14,15] or solid residues from sewage sludge gasification [16]. Scanning electron microscopy (SEM) coupled to energy dispersion spectrometry (EDS) and electron probe microanalysis (EPMA) are often used to determine the chemical compositions of various phases. The beam size of these techniques is generally close to 1 μm; however the volume of the analyzed material is generally in the range of several μm^3 according to the analytical conditions (beam current and beam accelerating voltage) and the nature of the specimen [17].

The general formula of the clinopyroxene (Cpx) is $M2M1T_2O_6$, where T is a tetrahedral site occupied mostly by Si and Al, whereas other cations enter the M2 and M1 sites [18 and references therein]. During our recent investigation of copper slags from the Zambian Copperbelt [12], we noticed the presence of potassium-rich Cpx. Potassium with ionic radius of 1.51 Å [19] was thought to be too large to enter the Cpx structure at ambient pressures. At higher pressures (>5 GPa), it was observed that potassium can substitute for Ca^{2+} or Mg^{2+} in the M2 site [18], which is, however, not possible for slags produced at ambient pressures. In this context, we carried out a more detailed study using a combination of other methods with significantly higher spatial resolution (focused ion beam technique coupled to transmission electron microscopy, FIB-TEM). Our data presented in this paper show how tricky the chemical determinations of phases in solid wastes can be, with particular implications and recommendations for the solid speciation of hazardous elements, such as metals and metalloids.

2. Experimental methods

The slag samples came from the Nkana slag dumps in the Zambian Copperbelt (S12°50′20″, E 28°12′40″) and occurred as heavy and dense fragments up to 7 cm in size of black to gray color. The

* Corresponding author. Tel.: +420 221951493; fax: +420 221951496.
E-mail address: ettler@natur.cuni.cz (V. Ettler).

0304-3894/$ – see front matter © 2012 Elsevier B.V. All rights reserved.
http://dx.doi.org/10.1016/j.jhazmat.2012.04.015

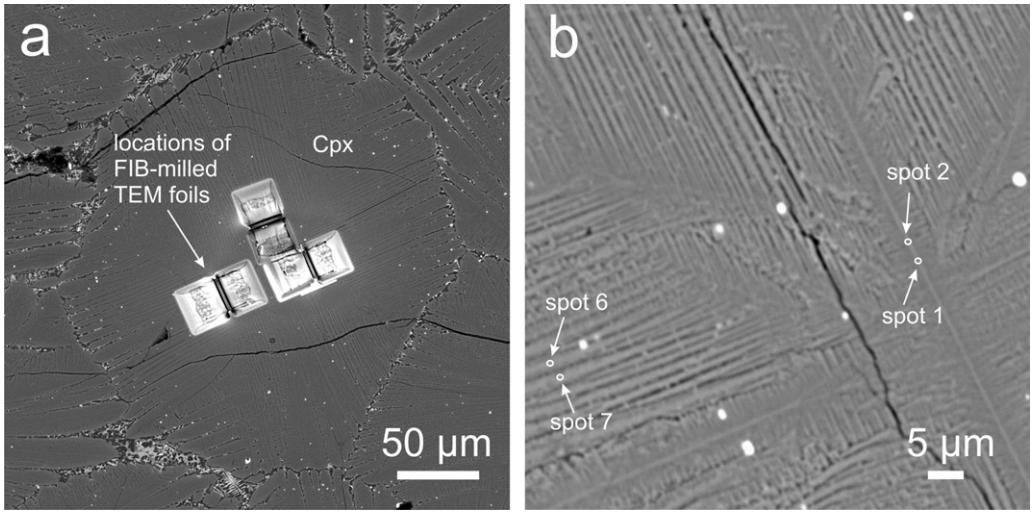

Fig. 1. SEM-BSE (back scattered electron) images (a) of clinopyroxene (Cpx) plumes and (b) zoom on individual Cpx lamellae from the Cu smelting slag with location of several EPMA spots.

samples were prepared as polished thin sections for microscopic observation and electron probe microanalysis. A TESCAN VEGA scanning electron microscope equipped with an Oxford Link X-Max 50 energy dispersion spectrometer at Charles University in Prague (Czech Republic) was used for imaging and semi-quantitative chemical analyses. Quantitative microanalyses were performed using a Cameca SX-100 electron microprobe (EPMA) at the Institute of Geology, Academy of Sciences of the Czech Republic, Prague. The following measurement conditions were used for the EPMA of silicate phases: accelerating voltage 15 kV, beam current 4 nA (low current used to avoid volatilization of alkalis), counting time 10 s and spot size 1 μm; standards used: jadeite, $NaAlSi_2O_6$ (Na, Kα), quartz, SiO_2 (Si, Kα), synthetic Al_2O_3 (Al, Kα), sanidine, (K,Na) $AlSi_3O_8$ (K, Kα), diopside, $CaMgSi_2O_6$ (Ca, Kα), rutile, TiO_2 (Ti, Kα), hematite, Fe_2O_3 (Fe, Kα), Mn—Cr spinel, $MnCr_2O_4$ (Cr, Kα), periclase, MgO (Mg, Kα), cobalt metal (Co, Kα). Empirical formulae of Cpx were calculated on 4 cations per formula unit and the ferric and ferrous iron contents were estimated assuming charge balance with 6 oxygens per formula unit.

To verify the presence of potassium in the Cpx at higher spatial resolution, three foils for transmission electron microscopy (TEM) have been prepared using a FEI Quanta 3D FEG Dual Beam focused ion beam (FIB) instrument at the Department of Lithospheric Sciences at the University of Vienna (Austria). The instrument is equipped with a Field Emission Gallium source. Platinum was used as deposition material for surface grounding and mounting the foil onto a Cu-grid. Throughout the sputtering and deposition processes, the ion-beam accelerating voltage was 30 kV, whereas successively lower beam currents (ranging from 50 nA to 30 pA) were used for progressive milling steps. Foils with dimensions of 17 μm × 10 μm × 2 μm were cut with a well-defined orientation perpendicular to the Cpx-lamellae. The foils were transferred to a Cu-grid by in-situ lift-out using an Omniprobe 100.7 micromanipulator. Then, the final thinning was performed stepwise using beam currents of 500 pA, 300 pA, 100 pA and finally 30 pA. The final thinned foil area was 13 μm × 9 μm in size and 90–160 nm thick. For subsequent TEM investigations presented in this paper, we used the thinnest area located close to the center of foil #2 with thickness close to 90 nm.

The TEM investigations on FIB-prepared foils were carried out on a JEOL JEM 3010 microscope operated at 300 kV (LaB_6 cathode, point resolution 1.7 Å) with an attached Oxford Instruments energy dispersive X-ray spectrometer (EDS) at the Institute of Inorganic Chemistry, Academy of Sciences of the Czech Republic. The images were recorded on a CCD camera with resolution of 1024 × 1024 pixels using the Digital Micrograph software package. The EDS analyses were acquired and treated in the INCA software package. Selected area electron diffraction (SAED) patterns were evaluated using the Process Diffraction software package [20].

3. Results and discussion

Previous studies using powder X-ray diffraction analysis (XRD), EPMA and SEM investigations indicated that Cpx and spinels were the predominant phases in the studied slags, often associated with minor olivine-type phases and leucite [12]. Whereas Cpx and olivines often formed large skeletal or harissitic crystals (up to several hundreds μm in size), leucite and spinels formed globular and well-delimited crystals, generally up to 100 μm in size [12]. In the slag sample, where K-Cpx was detected, Cpx forms approximately 1 mm wide, plume-shaped lamellar aggregates stacked in zones (Fig. 1a). Such spinifex textures indicate the quenching of the slag melt and rapid crystallization of Cpx. Individual Cpx crystallites were approximately 1–2 μm wide (Fig. 1b) and only larger lamellae were selected for the EPMA analyses. The EPMA indicate that the Cpx crystallites are enriched in K (Table 1). The maximum K concentration in Cpx was 2.88 wt% K_2O (corresponding to 0.146 atoms per formula units, *apfu*) in the core of lamellae of the plume-like crystals (spot 2, Fig. 1b). The EPMA of this KCpx yielded the formula $(Ca_{0.802}K_{0.146}Fe^{2+}_{0.030}Na_{0.020})_{\Sigma 1.000}(Fe^{2+}_{0.661}Fe^{3+}_{0.290}Mg_{0.226}Al_{0.100}Co_{0.042}Ti_{0.018})_{\Sigma 1.000}(Si_{1.742}Al_{0.258})_{\Sigma 2.000}O_{6.000}$.

However, the FIB-TEM investigation showed that Cpx lamellae are intimately associated with leucite ($KAlSi_2O_6$). Leucite inclusions of variable size (tens to hundreds of nm) and Cpx–leucite intergrowths were not visible on the SEM images, but were detected by TEM coupled to EDS and SAED (Fig. 2). EDS spot analyses as well as X-ray elemental mapping performed on the thinned foils indicate that K is not present in the clinopyroxene crystal structure but is exclusively related to the associated leucite (Fig. 2).

This study indicates that EPMA analyses provided the chemical compositions of Cpx, which are flawed due to the presence of nanometer-size solid inclusions and intergrowths with a K-rich phase (leucite), not clearly detectable during the SEM and EPMA work, but only in FIB-TEM foils (Figs. 1 and 2). Although the areas selected for EPMA looked homogeneous and were larger than the

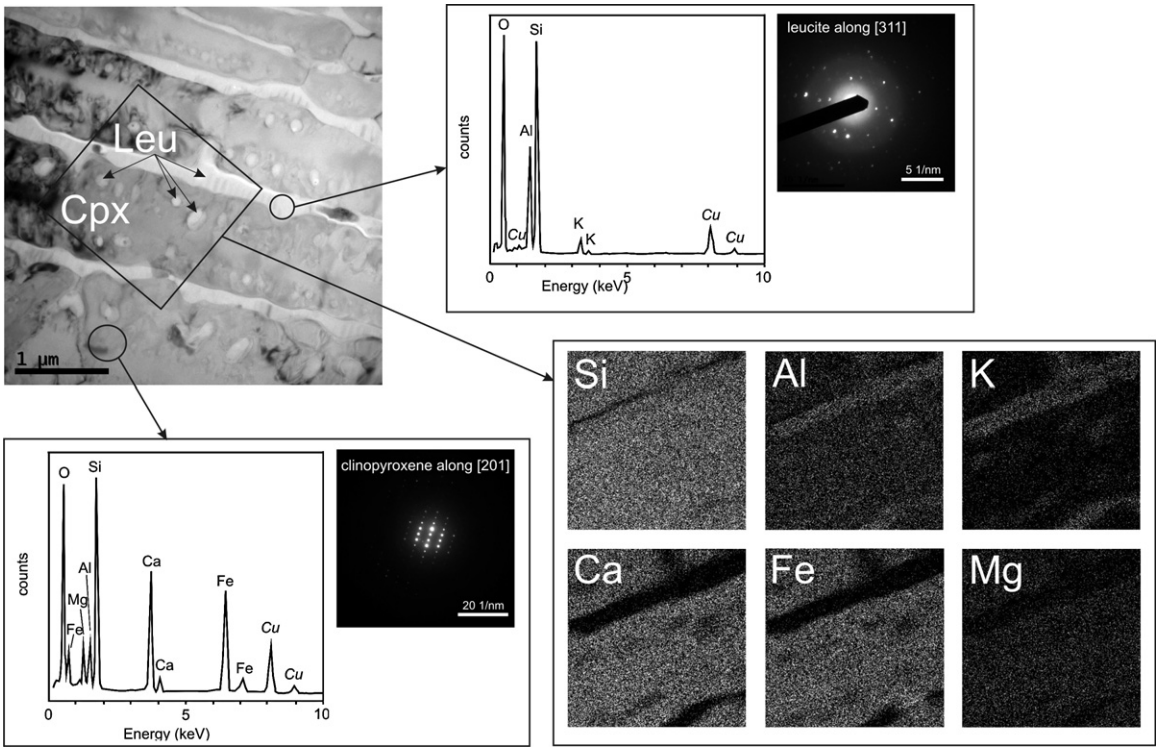

Fig. 2. TEM image of the FIB-prepared foil oriented perpendicular to the Cpx lamellae. The presence of leucite (Leu) trapped within the Cpx can be discerned. The individual phases were identified by SAED and EDS (Cu given in italics, being present in the TEM grid); the X-ray elemental maps show the spatial distribution of the major elements within a given zone.

Table 1
Representative electron microprobe analyses of plume-like clinopyroxenes (in wt% of oxides) and empirical formulae calculated to 4 cations and 6 oxygens per formula unit.

wt%	Spot 2	Spot 23	Range (n = 11)
SiO_2	43.73	44.54	43.15–44.54
TiO_2	0.59	0.61	0.54–0.7
Al_2O_3	7.63	7.84	6.42–7.84
Cr_2O_3	<DL	<DL	<DL-0.18
FeO	19.35	18.87	18.54–21.94
MgO	3.81	4.32	3.81–4.79
CoO	1.30	1.29	1.16–1.56
CaO	18.80	19.23	18.8–21.34
Na_2O	0.27	0.15	<DL-0.27
K_2O	2.88	1.98	0.62–2.88
Total	98.36	98.83	98.36–100.9
T site			
Si	1.742	1.765	1.705–1.765
$^{[4]}Al$	0.258	0.235	0.235–0.295
$^{[4]}Fe^{3+}$	n.d.	n.d.	n.d.
M1 site			
$^{[6]}Al$	0.100	0.132	0.014–0.132
$^{[6]}Fe^{3+}$	0.290	0.178	0.177–0.328
Ti	0.018	0.018	0.016–0.021
Cr	n.d.	n.d.	n.d.–0.006
Co	0.042	0.041	0.037–0.050
Mg	0.226	0.255	0.226–0.283
Fe^{2+}	0.325	0.376	0.323–0.400
M2 site			
Fe^{2+}	0.030	0.072	0.030–0.078
Ca	0.802	0.817	0.802–0.908
Na	0.021	0.012	n.d.–0.021
K	0.146	0.100	0.031–0.146

<DL – below detection limit; n.d. – not determined.

beam spot (1 μm), small leucite solid inclusions undetected during standard SEM imaging probably caused high K concentrations in the Cpx compositional data (Table 1). The leucite inclusions may have been invisible in SEM images due to their small grain size or due to their position immediately below the sample surface. In agreement with recently reviewed data on K-bearing clinopyroxene [18], it is improbable that K can enter the Cpx structure at ambient pressures.

Our results have significant implications, especially for the determination of chemical compositions of metal- and metalloid-bearing phases in hazardous waste materials. Standard SEM and EPMA have been routinely used in solid waste characterization over the past two decades. The recent literature contains a large number of papers showing how metals substitute for other cations in the crystalline phases and glass, which are often the predominant constituents of mineral solid wastes. In particular, numerous studies showed that glasses in smelting slags can contain significant amounts of metals. For example, Ettler et al. [2] reported up to 3.72 wt% PbO and 9.80 wt% ZnO in a matrix glass from Pb slags from Příbram, Czech Republic. Similarly, Piatak et al. [5] showed that interstitial glass in base-metal slags from smelting sites in the U.S.A. can contain up to 5.85 wt% PbO and 4.16 wt% ZnO. However, it is not clear whether these analyses correspond to the actual glass compositions or whether the samples were contaminated by admixtures of metal-rich nanophases. This aspect is very frequent in glasses due to the immiscibility between silicate and sulfide liquids, leading to late solidification of the metal-rich fraction within the residual glass. Another example of Pb smelting slag from Příbram (Czech Republic) is given to illustrate the difficulties associated with the EPMA reliability in waste characterization (Fig. 3a and b). The SEM microphotograph in backscattered electrons (BSE) shows metallic inclusions, significantly smaller than 1 μm, dispersed in glass (Fig. 3a and b). These can affect the chemical composition of the glass when analyzed by EPMA. Similarly, Seignez et al. [6] reported

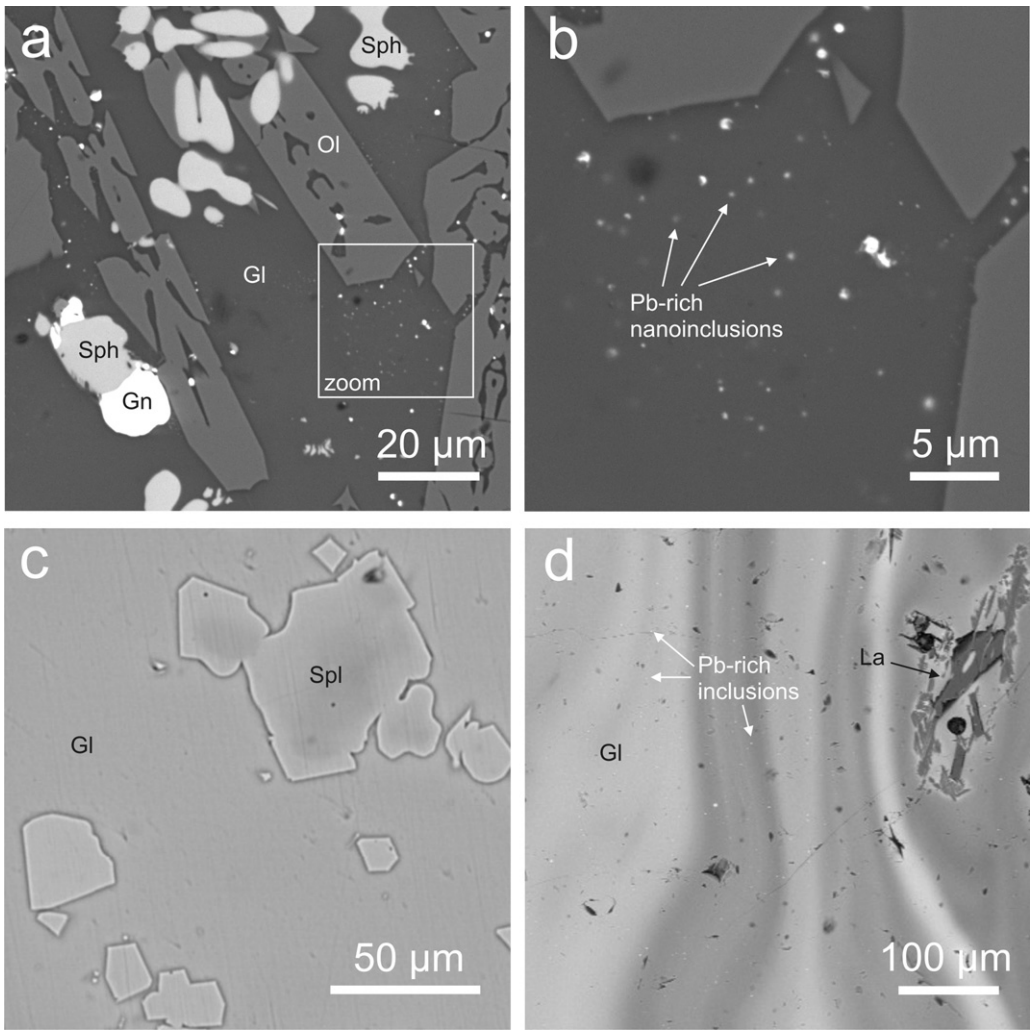

Fig. 3. SEM-BSE images of the base-metal smelting slags. (a) Typical assemblage of Pb slag composed of olivine (Ol), glass (Gl), sphalerite (Sph) and galena (Gn) (slag from Příbram, Czech Republic); (b) zoom on a glassy zone with nano-sized Pb-rich inclusions, which can affect the reliability of EPMA analyses of the glass; (c) metal-rich glass (7.85 wt% PbO, 9.12 wt% ZnO, 1.78 wt% CuO) with similar contrast as spinels (Spl) (slag from Tsumeb, Namibia, adapted from [10]); (d) difficult setting of contrast in an SEM image of Pb-rich glass (up to 33 wt% PbO) embedding small sulfide/metallic inclusions and associated to larnite, Ca_2SiO_4 (La) (medieval slag from an archaeological site in Prague, Czech Republic).

the presence of nanometer-scale phases (<60 nm) in glass from the Pb slag, probably corresponding to Fe oxides (wüstite, FeO), and also stressed that SEM/EDS and EPMA results must be interpreted with care. Consequently, these authors proposed the use of methods with higher resolution (TEM) in order to understand the effects of these nanophases on the leaching of contaminants related to the glass dissolution and other weathering processes [6,8].

The same feature is sometimes observed for crystalline phases. Indeed, submicron metal- and metalloid-bearing inclusions were also observed by numerous researchers within the early-crystallizing silicate and oxide phases [2,9,12] (see also Fig. 3a). Although it is known that some substituting elements can enter the structure of crystalline phases (e.g. Zn, Cr, Cu in spinels [2,12,13,21], Zn and Ni in olivines [2,3,9,10] and Zn in melilite [2,9,21]), it is not clear, however, to what extent the EPMA results can be flawed by the presence of nanophases. Melilite is known to contain high concentrations of Zn, corresponding to the hardystonite end-member, $Ca_2ZnSi_2O_7$ [21,22]. For example, in Zn-rich smelting slags from Poland, up to 23 wt% ZnO was reported in melilites [7]. Nevertheless, Bindi et al. [22] used TEM for the high-resolution investigation of natural Zn-rich melilite and found that the chemical composition in the sample can be slightly inhomogeneous on a nanoscale, showing the presence of a modulated structure inducing changes in diffraction patterns. Although small amounts of Pb are known to enter the melilite structure [22], it is nevertheless difficult to ascertain whether the reported high Pb concentrations in melilites from slags (up to 52.2 wt% PbO [7]) correspond to substitution in the crystal structure, and this is probably an artefact related to the presence of Pb-rich nanophases.

Investigation of secondary alteration products is even more complicated due to the complexity of weathering processes occurring at the waste-water interface. For example, Piantone et al. [15] reported that secondary calcite ($CaCO_3$) from weathered MSWI bottom ash can contain 0.82 ± 0.43 wt% PbO and up to 0.16 ± 0.19 wt% ZnO. Using EPMA, it is impossible to state whether these metals are incorporated into the calcite structure, adsorbed on the calcite surface, or simply form nano-sized impurities rich in cerussite ($PbCO_3$) or smithsonite ($ZnCO_3$) domains. Similarly, Bril et al. [23] studied the secondary alteration products on the surface of Zn slags from Poland and reported EPMA with high concentrations of Zn in anglesite ($PbSO_4$), barite ($BaSO_4$) and jarosite ($KFe_3(OH)_6(SO_4)_2$), which could correspond either to solid-solutions in some cases or to physical impurities.

4. Implication and recommendations

For mineralogical studies of solid waste materials, it is thus recommended that high-resolution SEM imaging be performed using modes that visualize compositional heterogeneities and to use a SEM instrument with high resolution capability, such as a field emission gun (FEG)-SEM. If a standard SEM instrument is used, particular care with different contrast setting is recommended. Despite their size (<1 μm) approaching the resolution limit of a standard SEM, it is relatively easy to visualize chemically contrasting entities trapped within the material with strikingly different mass (see e.g. metal-bearing droplets in silicate glass in Fig. 3a and b). In contrast, Fig. 3c and d shows more complicated situations with dense metal-rich glass having similar brightness to other associated heavy phases (spinel in Fig. 3c and minute sulfide/metallic droplets in Fig. 3d). In these cases, different contrast settings have to be consecutively employed to visualize all the phases present. As shown in this study, for polyphase materials with grain sizes on a scale of a few micrometers or less, the additional application of TEM, partly coupled to FIB sample preparation, is required in order to obtain reliable compositional information. It is nevertheless important to stress that artefacts of EPMA due to the limited spatial resolution caused by an interaction volume of several μm^3 in size can have a significant impact on modelling of the overall hazardous properties of the particular waste material (e.g., long-term leaching/release of contaminants) and, in justified cases, the solid speciation of contaminants should be verified by other methods with higher resolution (e.g. FIB-TEM).

Acknowledgments

This study was supported by the Czech Science Foundation (GAČR 210/12/1413), the Ministry of Education, Youth and Sports of the Czech Republic (MSM 0021620855), the Academy of Sciences of the Czech Republic (AV0Z30130516), the Austrian Science Fund (FWF, project I471-N19) and Charles University Student Project (SVV 263203). A number of colleagues helped with the microprobe techniques: Dr. Radek Procházka and Dr. Martin Racek (SEM/EDS), ing. Anna Langrová (EPMA). Dr. Madeleine Štulíková is thanked for correction of the English in the manuscript. The reviews of three anonymous reviewers helped significantly to improve the original version of the manuscript.

References

[1] P. Piantone, Mineralogy and pollutant-trapping mechanisms, C. R. Geosci. 336 (2004) 1415–1416.
[2] V. Ettler, O. Legendre, F. Bodénan, J.C. Touray, Primary phases and natural weathering of old lead-zinc pyrometallurgical slag from Příbram, Czech Republic, Can. Mineral. 39 (2001) 873–888.
[3] A. Manasse, M. Mellini, C. Viti, The copper slags of the Capattoli Valley, Campiglia Marittima, Italy, Eur. J. Mineral. 13 (2001) 949–960.
[4] V. Ettler, Z. Johan, Mineralogy of metallic phases in sulphide matte from primary lead smelting, C. R. Geosci. 335 (2003) 1005–1012.
[5] N.M. Piatak, R.R. Seal I.I., J.M. Hammarstrom, Mineralogical and geochemical controls on the release of trace elements from slag produced by base- and precious-metal smelting at abandoned mine sites, Appl. Geochem. 19 (2004) 1039–1064.
[6] N. Seignez, A. Gauthier, D. Bulteel, M. Buatier, P. Recourt, D. Damidot, J.L. Potdevin, Effect of Pb-rich and Fe-rich entities during alteration of a partially vitrified metallurgical waste, J. Hazard. Mater. 149 (2007) 418–431.
[7] J. Puziewicz, K. Zainoun, H. Bril, Primary phases in pyrometallurgical slags from a zinc-smelting waste dump, Świętochłowice, Upper Silesia, Poland, Can. Mineral. 45 (2007) 1189–1200.
[8] N. Seignez, A. Gauthier, D. Bulteel, D. Damidot, J.L. Potdevin, Leaching of lead metallurgical slags and pollutant mobility far from equilibrium conditions, Appl. Geochem. 23 (2008) 3699–3711.
[9] J. Kierczak, C. Néel, J. Puziewicz, H. Bril, The mineralogy and weathering of slag produced by the smelting of lateritic Ni ores, Szklary, southwestern Poland, Can. Mineral. 47 (2009) 557–572.
[10] V. Ettler, Z. Johan, B. Kříbek, O. Šebek, M. Mihaljevič, Mineralogy and environmental stability of slags from the Tsumeb smelter, Namibia, Appl. Geochem. 24 (2009) 1–15.
[11] V. Ettler, R. Červinka, Z. Johan, Mineralogy of medieval slags from lead and silver smelting (Bohutín, Příbram district, Czech Republic): towards estimation of historical smelting conditions, Archaeometry 51 (2009) 987–1007.
[12] M. Vítková, V. Ettler, Z. Johan, B. Kříbek, O. Šebek, M. Mihaljevič, Primary and secondary phases in copper–cobalt smelting slags from the Copperbelt Province, Zambia, Mineral. Mag. 74 (2010) 581–600.
[13] N.M. Piatak, R.R. Seal I.I., Mineralogy and the release of trace elements from slag from the Hegeler Zinc smelter, Illinois (USA), Appl. Geochem. 25 (2010) 302–320.
[14] P. Piantone, F. Bodénan, R. Derie, G. Depelsenaire, Monitoring the stabilization of municipal solid waste incineration fly ash by phosphation: mineralogical and balance approach, Waste Manage. 23 (2003) 225–243.
[15] P. Piantone, F. Bodénan, L. Chatelet-Snidaro, Mineralogical study of secondary mineral phases from weathered MSWI bottom ash: implications for the modelling and trapping of heavy metals, Appl. Geochem. 19 (2004) 1891–1904.
[16] A.B. Hernandez, J.H. Ferrasse, P. Chaurand, H. Saveyn, D. Borschneck, N. Roche, Mineralogy and leachability of gasified sewage sludge solid residues, J. Hazard. Mater. 191 (2011) 219–227.
[17] P.J. Potts, J.F.W. Bowles, S.J.B. Reed, M.R. Cave, Microprobe Techniques in the Earth Sciences, in: The Mineralogical Society Series 6, Chapman & Hall, London, 1995.
[18] O.G. Safonov, L. Bindi, V.L. Vinograd, Potassium-bearing clinopyroxene: a review of experimental, crystal chemical and thermodynamic data with petrological applications, Mineral. Mag. 75 (2011) 2467–2484.
[19] R.D. Shannon, Revisd effective ionic radii and systematic studies of interatomic distances in halides and chalcogenides, Acta Cryst. 32 (1976) 751–767.
[20] J.L. Lábár, Consistent indexing of a (set of) SAED pattern(s) with the Process Diffraction program, Ultramicroscopy 103 (2005) 237–249.
[21] A. Trujillo-Vazquez, H. Metiver-Pignon, L. Tiruta-Barna, P. Piantone, Characterization of a mineral waste resulting from the melting treatment of air pollution control residues, Waste Manage. 29 (2009) 530–538.
[22] L. Bindi, M. Czank, F. Röthlisberger, P. Bonazzi, Hardystonite from Franklin Furnace: a natural modulated melilite, Am. Mineral. 86 (2001) 747–751.
[23] H. Bril, K. Zainoun, J. Puziewicz, A. Courtin-Nomade, M. Vanaecker, J.C. Bollinger, Secondary phases from the alteration of a pile of zinc-smelting slags as indicators of environmental conditions. An example from Świętochłowice, Upper Silesia, Poland, Can. Mineral. 46 (2008) 1235–1248.